Published in final edited form as:
Concepts Magn Reson Part B Magn Reson Eng. 2010 April 1; 37B(2): 65–74. doi:10.1002/cmr.b.20159.

Quantitative Comparison of Minimum Inductance and Minimum Power Algorithms for the Design of Shim Coils for Small Animal Imaging

PARISA HUDSON, **STEPHEN D. HUDSON**, **WILLIAM B. HANDLER**, **TIMOTHY J. SCHOLL**, and **BLAINE A. CHRONIK**
Department of Physics and Astronomy, University of Western Ontario, London, ON, Canada

Abstract

High-performance shim coils are required for high-field magnetic resonance imaging and spectroscopy. Complete sets of high-power and high-performance shim coils were designed using two different methods: the minimum inductance and the minimum power target field methods. A quantitative comparison of shim performance in terms of merit of inductance (ML) and merit of resistance (MR) was made for shim coils designed using the minimum inductance and the minimum power design algorithms. In each design case, the difference in ML and the difference in MR given by the two design methods was <15%. Comparison of wire patterns obtained using the two design algorithms show that minimum inductance designs tend to feature oscillations within the current density; while minimum power designs tend to feature less rapidly varying current densities and lower power dissipation. Overall, the differences in coil performance obtained by the two methods are relatively small. For the specific case of shim systems customized for small animal imaging, the reduced power dissipation obtained when using the minimum power method is judged to be more significant than the improvements in switching speed obtained from the minimum inductance method.

Keywords

shim coils; MRI; target field; minimum inductance target field; minimum power target field

INTRODUCTION

A high-field clinical magnetic resonance imaging (MRI) scanner, such as a 3 T scanner, has the potential to operate with a high signal-to-noise ratio, allowing the acquisition of high-quality magnetic resonance spectroscopy (MRS) data and high-resolution MR images, provided that the field inhomogeneities are well shimmed (1). At higher magnetic field, field inhomogeneities can be larger, resulting in phase and frequency instability in MRI signals and line broadening and frequency shifts in MRS (1,2). To correct the larger field inhomogeneities, gradient and shim coils with higher performance than those available in typical clinical MRI scanners are required. High-performance gradient and shim coils require low inductance (L) to allow short switching times, low resistance (R) to minimize power dissipation, and high efficiency (η) to produce the desired field (3). However, when designing high-performance coils, the trade-offs between different coil characteristics

Correspondence to: Dr. Blaine A. Chronik; bchronik@uwo.ca.

should be considered. For example, minimum inductance coil designs allow faster switching speeds while minimum power coil designs optimize the power consumption.

A target-field approach for designing gradient coils was devised by Turner (4). His method relies on inverse Fourier transformations to determine a continuous current distribution, confined to flow on cylindrical shells or on planes that yields the desired field. With this method, a functional that includes the deviation of the desired field from the calculated field over the region of interest (ROI) is formed. The current density in the reciprocal domain is found by minimizing the functional with respect to the current density. Turner further developed the target field method by adding inductance to the functional (5). This minimized the inductance while maintaining a specified field over the desired ROI.

Carlson et al. (6) modified Turner's inductance minimization technique by expanding the current density as a sum of truncated sinusoidal functions, allowing the length of gradient coils to be constrained. Bowtell and Robyr (7) allowed the current density to vary in the radial direction in addition to the axial and azimuthal directions, for the design of multilayer, cylindrical gradient coils. In their design algorithm, power and inductance of the coil were minimized simultaneously. Further developments were made by Forbes and Crozier in a series of papers (8–10), for the design of shielded zonal and tesseral shim coils on cylindrical and planar surfaces.

Poole and Bowtell (11) applied the boundary element method to design gradient coils wound on arbitrarily shaped surfaces, by discretizing the current density into a mesh of triangles. The inductance, resistance, and torque were derived in terms of current density, allowing for a functional capable of simultaneously minimizing the square of the difference between the target field and the actual field, the stored energy, the power loss, and the torque exerted on the coils.

As mentioned, many methods have been developed for the design of gradient and shim coils. These methods are able to minimize properties such as power and inductance, allowing coils to be optimized for a variety of applications in MRI and MRS. In an International Society of Magnetic Resonance for Medicine proceeding, Turner reported on the comparison of gradient coil performance for coils designed using the minimum inductance and minimum power methods (12). To the best of the authors' knowledge, no quantitative comparison of minimum inductance and minimum power design algorithms has been published for a shim coil set designed for small animal imaging.

In this article, the method of Turner was applied to design high-order shim sets containing 10 independent axes. The shim sets were designed using both minimum inductance and minimum power algorithms, and a quantitative comparison was made between coil performances obtained with the two methods. These quantitative comparisons are critical first steps for the optimization of practical, high-power, high-order shim sets, designed for MRI and MRS applications in small animals.

THEORY

For the design of the cylindrical shims used in MRI, the axial component of the magnetic field, $B_z(\rho, \varphi, z)$, is of interest. For a current constrained to flow on a surface of a cylinder, only the azimuthal component of the current density, $J_\varphi(\varphi,z)$, contributes to the axial component of the magnetic field. Inside a coil of radius a (i.e., in the region where $\rho < a$), the axial component of the magnetic field can be represented in terms of cylindrical harmonics (13,14):

$$B_z(\rho,\varphi,z) = -\mu_0 a \sum_{m=-\infty}^{\infty} \int_{-\infty}^{\infty} dk e^{im\varphi} e^{i2\pi kz} j_\varphi^m(k) |k| I_m \times (|2\pi k\rho|) K_m'(|2\pi ka|), \quad [1]$$

where I_m and K_m' are the modified Bessel functions (15,16) and K_m' is the derivative of K_m which can be written as $K_m' = \frac{-1}{2}(K_{m+1} + K_{m-1})$. The Fourier transform of the azimuthal component of current density is given by:

$$j_\varphi^m(k) = \int_{-\pi}^{\pi} d\varphi e^{-im\varphi} \int_{-\infty}^{\infty} dz e^{-i2\pi kz} J_\varphi(\varphi, z). \quad [2]$$

Our goal is to find an optimal current density, $j_\varphi^m(k)$, to achieve a desired magnetic field in the ROI, as well as to minimize some physical parameters of the coil (such as inductance or power dissipation). Considering these requirements, we introduce a functional, $U\{j_\varphi^m(k)\}$, that consists of two terms:

$$U\left\{j_\varphi^m(k)\right\} = Z\left\{j_\varphi^m(k)\right\} + \sum_{n=1}^{N} \lambda_n [B_z(\rho_n, \varphi_n, z_n) - B_{zn}], \quad [3]$$

where B_{zn} are the desired z-components of the magnetic field at the target points, N is the number of field targets, λ_n are the Lagrange multipliers (5), and Z is the physical characteristic of the coil that should be minimized. For example Z could be power, inductance, or their combination.

To minimize a physical parameter of the coil, it must be expressed in terms of the current density. For designing coils with minimized inductance, inductance is represented in terms of the current distribution over the coil by (3,5):

$$L = \frac{-\mu_0 a^2}{2\pi I^2} \sum_{m=-\infty}^{\infty} \int_{m=-\infty}^{\infty} dk \left| j_\varphi^m(k) \right|^2 I_m'(|2\pi ka|) K_m'(|2\pi ka|), \quad [4]$$

where I is the current required to produce the current surface density.

If minimum power designs are desired, power dissipation resulting from a current density flowing on the surface of a cylinder of thickness t and resistivity ρ can be expressed as (3,5):

$$P = \frac{\rho a}{2\pi t} \sum_{m=-\infty}^{\infty} \int_{-\infty}^{\infty} dk \left| j_\varphi^m(k)^2 \right| \left(1 + \frac{m^2}{(2\pi ka)^2}\right). \quad [5]$$

As both inductance and power are quadratic in $j_\varphi^m(k)$ (Eqs. [4] and [5]), absolute minima of inductance and power are attainable. These minima, subject to the field constraints, are found when:

$$\frac{dU\left(j_{\varphi}^{m}(k)\right)}{dj_{\varphi}^{m}(k)}=0. \quad [6]$$

This gives an expression relating $j_{\varphi}^{m}(k)$ and λ which can be substituted back into Eq. [1], allowing B_z to be written in terms of λ. Substituting this expression for B_z into:

$$B_z(\rho_n, \varphi_n, z_n) - B_{zn}=0, \quad [6]$$

gives a set of linearly independent equations that can be assembled into a matrix equation and solved for the set of $\{\lambda_n\}$ using singular value decomposition. The matrix has dimensions $N \times N$, where N is the number of field targets. Having the set of $\{\lambda_n\}$, the current density can be derived over the surface of the coil via substitution. The complete derivation for the minimum inductance method has been shown by Turner (5) and Chronik and Rutt (17). The complete derivation for the minimum power method is presented in Appendix A.

Optimum accuracy of the magnetic field and the resistance would be achieved by building a coil with a continuous current density. In practice, it is only possible to build a coil that approximates the continuous current density. The current density was approximated with a finite set of current carrying loops. To determine the loops position under the condition $\nabla . J = 0$, we define a stream function, S(z), that corresponds to the surface current density, $J_{\varphi}(\varphi, z)$, (18) as:

$$S(z)=\int_{-z}^{z} J_{\varphi}(\varphi, z')dz'. \quad [4]$$

The stream function is discretized into some contours using the contouring function of Matlab version 7.5 (The Mathworks, Natick, MD). Contours were found at a fixed number of values (levels) of the stream function. The contours of the stream function are the discrete wire patterns that approximate the continuous current density. Wires were positioned along the contours of the stream function and each contour represents one or more closed loops on the cylindrical surface of the coil (18).

METHODS

The calculations and design algorithms were implemented in Matlab version 7.5. The following 10 separate gradient and shim axes were designed using both the minimum inductance and the minimum power methods: X, Y, Z, XY, $X^2–Y^2$, YZ, XZ, Z^2, Z^3, and Z^4. For the remainder of this discussion, all of these will be referred to as shim coils (i.e., gradient coils will be considered as first-order shims). All coils were designed with a radius of 10 cm.

For each axis, identical magnetic field constraints were used for both the minimum inductance and the minimum power methods. The magnetic field was specified at nine evenly spaced points, between $z = \pm 0.5a$ where a is the radius of the coil, parallel to the z-axis. Increasing the number of field constraints over the same region increases both the accuracy of the field and the size of the region of uniformity, at the expense of coil efficiency. For zonal axes, the field targets were located on the z-axis, with the appropriate pure polynomial variation with z, and for tesseral axes, the field targets were offset from the z-axis by $0.5a$ at an angle of zero radians. Using field targets at multiple radial locations did not significantly affect the design of tesseral coils. The current density of tesseral axes were

found by limiting the expansion to have only the azimuthal order necessary for that shim; for the first-order shims we included only $m = \pm 1$ in the current density expansion, for the second-order shims we included only $m = \pm 2$, etc. (see Appendix).

The continuous current density was approximated as loops of current carrying wire. The location of wire was determined from contours of the stream function using the Matlab contouring function. Once the wire pattern was obtained, it was discretized into an array of elements characterized by their positions and lengths, each carrying current *I*. The magnetic field generated by each coil was calculated using the elemental Biot-Savart equation on the array of wire elements (14). For each coil, it was verified that the numerically calculated field met the field targets. Coils designed with the two methods were compared using inductive merit (ML) and resistive merit (MR).

ML and MR were calculated with both discrete and continuous methods. For the discrete method, inductance was evaluated by applying the Neumann formula (13,14) to the wire element array.

Resistance was calculated by summing the resistances of the wire elements in the element array. In the case of rectangular wire, the radial thickness of the conducting layer used for coil fabrication was assumed to be constant and the width of the conducting path was assumed to be equal to the minimum spacing. The cross-sectional area of each wire element would then be the thickness multiplied by the minimum spacing. If round wire were considered, the cross-sectional area would be the area of a circle with a diameter equal to the minimum spacing.

Regardless of the cross-section of a discrete wire, efficiency varies linearly with the number of loops while inductance varies quadratically. Using this information, an equation for ML independent of the number of loops was created. ML is defined as $\frac{\eta}{L^{1/2}}$ where *L* is the coil inductance and η is the field efficiency of the coil (7).

To develop a figure of merit for resistance or power, the dependence of resistance on the number of loops must first be determined for the cases of rectangular and circular cross-section wires separately. The wire length increases linearly with the number of loops for both rectangular and round wires. The cross-sectional area of round wire (π multiplied by one-half the minimum spacing squared) is inversely proportional to the number of loops squared because the minimum spacing is proportional to the number of loops. Combining these two effects, the coil resistance (*R*) for round wire is found to vary as the third power of the number of loops. For rectangular wire, the thickness is held constant, and therefore the cross-sectional area (thickness multiplied by the minimum spacing) is inversely proportional to the number of loops. This causes the coil resistance for rectangular wire to vary with the number of loops. To obtain a MR equation independent of the number of loops, MR was therefore defined as $\frac{\eta}{R^{1/2}}$ for rectangular wire and $\frac{\eta}{R^{1/3}}$ for round wire (7). The coil radius is not included in the merit equations for this work because it was held constant for coils designed with both the minimum inductance and the minimum power methods.

For the continuous method, the continuous current density was directly substituted into equations for magnetic field, inductance, and power (3). As with the discrete method, mathematical functions were fit to the analytical calculated field to obtain the efficiencies of the individual shim coils.

ML and MR were calculated for the minimum power and the minimum inductance designs with both discrete and continuous methods. Absolute field residuals, defined as the difference between the actual field and the assumed ideal shape of the field (i.e., the

difference between the field created by the shim and the fitted field profile), were calculated inside a cylindrical volume with a radius of 0.9*a* and a length of 1.8*a* (approximately six times the volume of the ROI). Relative field residuals, defined as the percent difference between the actual field and the assumed ideal shape of the field were also calculated in the same region. Relative field residuals were not calculated where the value of the ideal function used to describe the shape of the field was expected to be equal to zero. Both absolute and relative field residuals were calculated for all shim axes as a method of characterizing field uniformity.

RESULTS AND DISCUSSION

Figure 1 shows the upper halves of the Z^2 wire patterns and Fig. 2 shows the upper halves of the $X^2–Y^2$ wire patterns created using a) the minimum inductance and b) the minimum power design algorithms. The bottom halves of the coils are mirror images of the top halves. Both algorithms prevent current density from spreading out indefinitely over the coil surface. The basic features characteristic of the two methods are apparent: minimum inductance designs tend to feature oscillations within the current density and minimum power designs tend to feature longer, less rapidly varying current densities, and lower power dissipation. These features are consistent across all shim axes designed using these two methods.

Figure 3(a) illustrates the calculated magnetic field profile and the field targets versus *z* for the Z^2 coil. Within the ROI (the cylinder of length *a* and radius 0.5*a*), the field profile, having a relative error of 10^{-6}, shows negligible deviation from the field targets, and the quadratic behavior of the magnetic field continues well outside the ROI. The field profile for an $X^2–Y^2$ shim coil, calculated in the *xy* plane within the ROI, is shown in Fig. 3(b). The magnetic field deviates from the $x^2–y^2$ behavior more quickly than for the Z^2 coil.

The field profiles given by the two design methods are almost identical within the ROI. However, small differences can be measured by comparing the relative residual fields given by each method. The relative and absolute residual fields for the $X^2–Y^2$ coils are shown in the *xy* plane and the *yz* plane in Figs. 4 and 5, respectively. In each figure, subfigures a and c show the relative and absolute residual fields for the minimum inductance design, respectively, and sub-figures b and d show the relative and absolute residual fields for the minimum power design, respectively. Due to symmetry, only one quadrant of the relative residual fields is shown. For all tesseral coils, the average relative field residuals are <2% and the average absolute field residuals are $<10^{-7}$ T in the *xy* plane within the ROI, when evaluated using both design methods. In the *yz* plane within the ROI, the average relative residual fields are <4% and the average absolute residual fields are $<10^{-6}$ T for all tesseral coils made with both design methods. For all zonal coils made with both design methods, the average relative residual fields are <2% and the average absolute residual fields are $<10^{-8}$ T in the *yz* plane within the ROI. The magnetic fields produced by the coils designed using the minimum power and the minimum inductance methods are scaled to have the same efficiency.

Table 1 summarizes the ML and MR values for the 10 different shim axes. Percent differences of the merits of inductance and of the merits of resistance were calculated for coils designed with the minimum power and the minimum inductance methods. The absolute values of MR and ML cannot be compared between different shim axes; however, they can be used to compare designs for any given shim axis. In all cases, regardless of discrete or continuous evaluation, coils designed using the minimum inductance method have higher ML values, while coils designed using the minimum power method have higher MR values, as expected. However, it is equally clear that the differences between the design

algorithms are small. When the stream functions were sampled with the same number of levels, the improvement in ML provided by the minimum inductance method is <10% of the value obtained using the minimum power method, in every design case. The improvements in MR provided by the minimum power method are <15% of the values obtained using the minimum inductance method. When the stream function sampling levels were adjusted to achieve constant coil efficiency, the improvements are 10–20% in ML and 20–30% in MR for the minimum inductance method and the minimum power method, respectively.

The ML calculated with the discrete method agrees with the ML calculated with the continuous method within 3.5% in all cases. This is expected because both efficiency and inductance are independent of current density. The difference between the merits of power calculated with the discrete and the continuous methods ranges between 10% and 30%. This larger discrepancy is observed because the resistance calculated by the discrete method is higher than the one calculated by the continuous method.

The results summarized in Table 1 are specific to the particular case of 10-cm radius shim coils that correct for field inside an imaging region of 10 cm. The radii of the coils were chosen to be twice the radius of the imaging region. More work is required to extend these results to shim coil axes designed over a wider range of uniformity parameters.

To relate the results of this study to pulse sequence parameters for a simple example MRI pulse sequence, the effect of readout-gradient performance on a fast gradient echo sequence was simulated. The amplifier parameters were as follows: maximum voltage of 1,200 V, maximum current of 400 A. The acquisition parameters were receiver bandwidth of 125 kHz, 256 k-space data points along the readout direction, and field of view equal to 10 cm. Gradient coils from both methods were scaled to have equal efficiency of 1.38 mT/m/A. The gradient coil designed using the minimum inductance method allowed a minimum TE of 1.13 ms and a dissipated RMS power of 512 W, whereas the gradient coil designed using the minimum power method allowed a minimum TE of 1.15 ms and a dissipated RMS power of 410 W. In this case then, the minimum inductance method results in a decrease of the minimum echo time of <2%, while the minimum power method results a decrease in power dissipation of 22%. For this application, it is probably most advantageous to utilize the minimum power design.

In this study, it has been shown that for shims coils of higher orders, minimum power algorithms yield coils with approximately 30% reduced power dissipation as compared to minimum inductance algorithms; while minimum inductance algorithms yield coils with approximately 20% reduced switching times. The question becomes: which is more significant for MRI applications? In the opinion of the authors, for small animal imaging studies at high field, the reduction in switching times provided by minimum inductance coil designs is not significant compared to the reduction in power dissipation allowed by minimum power designs. Modern imaging pulse sequences employing steady-state methods typically require gradients operating at high strength with very high duty cycles, where power dissipation is the primary limitation. Furthermore, high-power shimming essentially requires direct current operation of the shim coils, and as shimming requirements increase, the thermal dissipation within the shim set is also expected to limit operation. Regardless, the results of this study allow judgments regarding gradient and shim coil design algorithm to be made on an informed, application-specific basis.

References

1. Li BS, Regal J, Gonen O. SNR versus resolution in 3D 1H MRS of the human brain at high magnetic fields. Magn Reson Med 2001;46:1049–1053. [PubMed: 11746567]

2. Barker PB, Hearshen DO, Boska MD. Single-voxel proton MRS of the human brain at 1.5 T and 3.0 T. Magn Reson Med 2001;45:765–769. [PubMed: 11323802]
3. Turner R. Gradient coil design—a review of methods. Magn Reson Med 1993;11:903–920.
4. Turner R. A target field approach to optimal coil design. J Phys [D] 1986;19:L147–L151.
5. Turner R. Minimum inductance coils. J Phys [E] 1988;21:948–995.
6. Carlson JW, Derby KA, Hawryszko KC, Weideman M. Design and evaluation of shielded gradient coils. Magn Reson Med 1992;26:191–206. [PubMed: 1513247]
7. Bowtell R, Robyr P. Multilayer gradient coil design. J Magn Reson 1998;131:286–294. [PubMed: 9571104]
8. Forbes LK, Crozier S. A Novel target-field method for finite-length magnetic resonance shim coils: I. zonal shims. J Phys [D] 2001;34:3447–3455.
9. Forbes LK, Crozier S. A Novel target-field method for finite-length magnetic resonance shim coils: II. tesseral shims. J Phys [D] 2002;35:839–849.
10. Forbes LK, Crozier S. A Novel target-field method for magnetic resonance shim coils: III. shielded zonal and tesseral coils shims. J Phys [D] 2003;36:68–80.
11. Poole M, Bowtell R. Novel gradient coil designed using a boundary element method. Concept Magn Reson [B] 2007;31B:162–175.
12. Turner, R. Comparison of Minimum Inductance and Minimum Power Gradient Coil Design Strategies. Berkeley, CA: 1992. p. 4031
13. Jackson, JD. Classical Electrodynamics. New York: John Wiley & Sons; 1998.
14. Reitz, JR.; Milford, FJ.; Christy, RW. Foundation of Electromagnetic Theory. New York: Addison Wesley; 1989.
15. Hildebrand, FB. Advanced Calculus for Applications. Prentice-Hall; 1976.
16. Abramowitz, M.; Stegan, IA. Hand Book of Mathematical Functions. New York: Dover; 1965.
17. Chronik BA, Rutt BK. Constrained length minimum inductance gradient coil design. Magn Reson Med 1998;39:270–278. [PubMed: 9469710]
18. Peeren GN. Stream function approach for determining optimal surface current. J Comp Phys 2003;191:305–321.

APPENDIX

To complete the derivation of the current density for the minimum power method, the *z*-component of the magnetic field should be expanded in cylindrical harmonics using the Green's function theory (13):

$$B_z(\rho,\varphi,z) = -\mu_0 a \sum_{m=-\infty}^{\infty} \int_{-\infty}^{\infty} dk e^{im\varphi} e^{i2\pi kz} j_\varphi^m(k) |k| I_m \times (|2\pi k\rho|) K_m'(|2\pi ka|), \quad [A1]$$

where a is the radius of the coil. I_m and K_m are the modified Bessel functions. The power dissipation in the coil can also be expanded in cylindrical harmonics (3):

$$P = \frac{\rho a}{2\pi t} \sum_{m=-\infty}^{\infty} \int_{-\infty}^{\infty} dk \left| j_\varphi^m(k) \right|^2 \left(1 + \frac{m^2}{(2\pi ka)^2} \right), \quad [A2]$$

where ρ is the resistivity and t is the thickness of the conductor. The functional, $U\{j_\varphi^m(k)\}$, consists of power, $P\{j_\varphi^m(k)\}$, and the field constraints deviation from the calculated field:

$$U\left\{j_{\varphi}^{m}(k)\right\}=P\left\{j_{\varphi}^{m}(k)\right\}+\sum_{n=1}^{N}\lambda_{n}[B_{z}(\rho_{n},\varphi_{n},z_{n})-B_{zn}]. \quad [A3]$$

B_{zn} are the z-components of the desired magnetic field and λ_n are Lagrange multipliers. The minimum value of P, subject to the field constraints, is given when:

$$\frac{dU\left\{j_{\varphi}^{m}(k)\right\}}{dj_{\varphi}^{m}(k)}=0. \quad [A4]$$

Taking the derivative of U with respect to the reciprocal current density, $j_{\varphi}^{m}(k)$, setting it equal to zero, and solving for $j_{\varphi}^{m}(k)$ yields:

$$j_{\phi}^{m}(k)=\sum_{n=1}^{N}\lambda_{n}a_{n}, \quad [A5]$$

where

$$a_{n}=\frac{\mu_{0}t\pi}{\rho}\frac{1}{\left(1+\frac{m^{2}}{(2\pi ka)^{2}}\right)}\times e^{im\varphi}e^{i2\pi kz}|k|I_{m}(|2\pi k\rho_{n}|)K_{m}^{\prime}(|2\pi ka|). \quad [A6]$$

Once the set of λ_n is known in Eq. [A5], Eq. [A6] gives the reciprocal current density, $j_{\varphi}^{m}(k)$. To find λ_n, the field constraint equations:

$$B_{z}(\rho_{n},\phi_{n},z_{n})-B_{zn}=0, \quad [A7a]$$

should be considered. Equation [A5] can be substituted back into Eq. [A1] to write B_z in terms of λ_n. Substituting this expression for B_z into Eq. [A7a] yields:

$$\left[-\mu_{0}a\sum_{n=1}^{N}\sum_{m=-\infty}^{\infty}\int_{-\infty}^{\infty}dke^{im\varphi}e^{i2\pi kz}\lambda_{n}a_{n}|k|I_{m}(|2\pi ka|)\times K_{m}^{\prime}(|2\pi ka|)\right]-B_{zn}=0. \quad [A7]$$

Equation [A7b] is a set of linearly independent equations that can be assembled into a matrix equation:

$$[M][\lambda_{n}]=[B_{zN}], \quad [A8]$$

and solved for the set of $\{\lambda_n\}$ using the singular value decomposition method. The elements of the matrix M are the integrals as a function of the constraint coordinates:

$$M(n,n')=\frac{-\pi\mu_0^2 ta}{\rho}\sum_{m=-\infty}^{\infty}\int_{-\infty}^{\infty}dk e^{im(\varphi_n+\varphi_{n'})}\times e^{i2\pi k(z_n+z_{n'})}\frac{|k|^2 I_m(|2\pi k\rho_n|)I_m(|2\pi k\rho_{n'}|)K_m'^2(|2\pi ka|)}{1+\frac{m^2}{(2\pi ka)^2}} \quad [A9]$$

Evaluating the elements of M using Eq. [A9], solving Eq. [A8] for the set of $\{\lambda_n\}$, and substituting λ_n's into Eq. [A5] gives the current density, $j_\varphi^m(k)$. The $J_\varphi(z,\varphi)$ can be calculated by taking the inverse transform of $j_\varphi^m(k)$. As the current density is known, Eqs. [1A] and [2A] give us the magnetic field and the power, respectively.

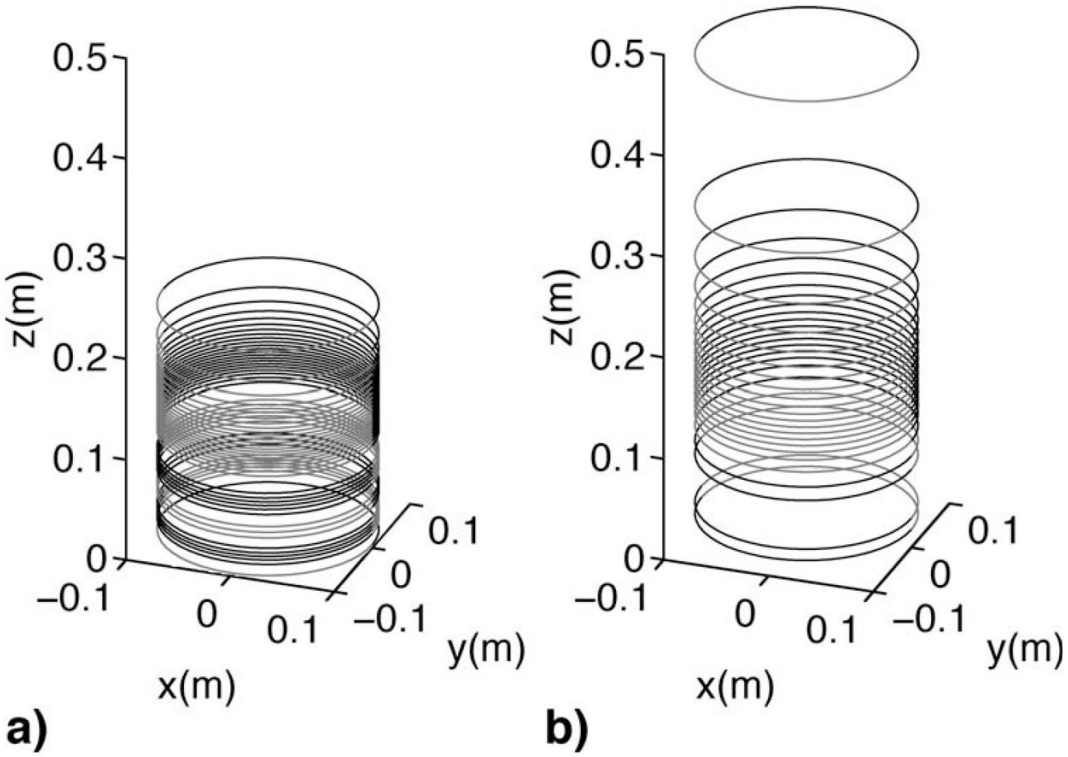

Figure 1.
The upper half ($z > 0$) of the Z^2 wire pattern given by (a) minimum inductance and (b) minimum power methods. The bottom halves of the coils are mirror images of the top halves not shown in this figure. Minimum power designs tend to feature longer, less compact wire patterns than minimum inductance designs.

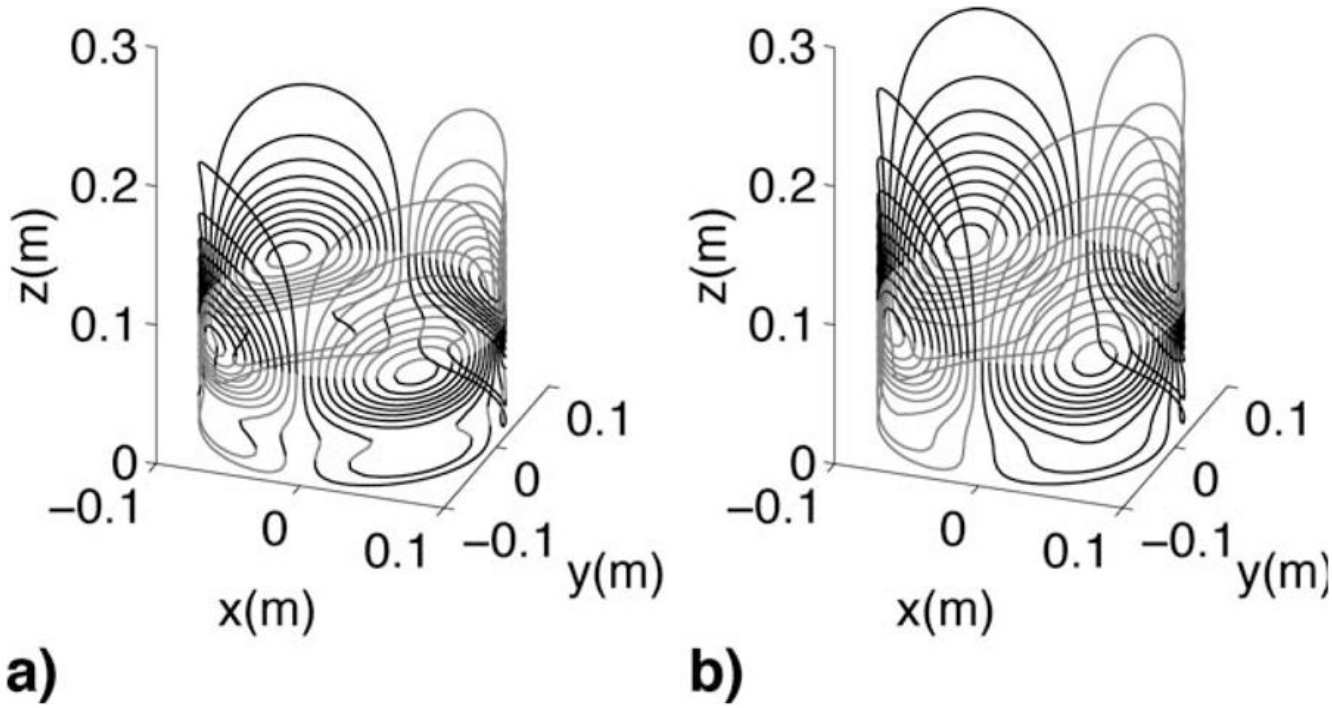

Figure 2.
The upper half ($z > 0$) of the X^2–Y^2 wire pattern given by (a) minimum inductance and (b) minimum power methods. The bottom halves of the coils are mirror images of the top halves not shown in this figure. Minimum inductance designs tend to give more complex wire and more compact wire patterns than minimum power designs.

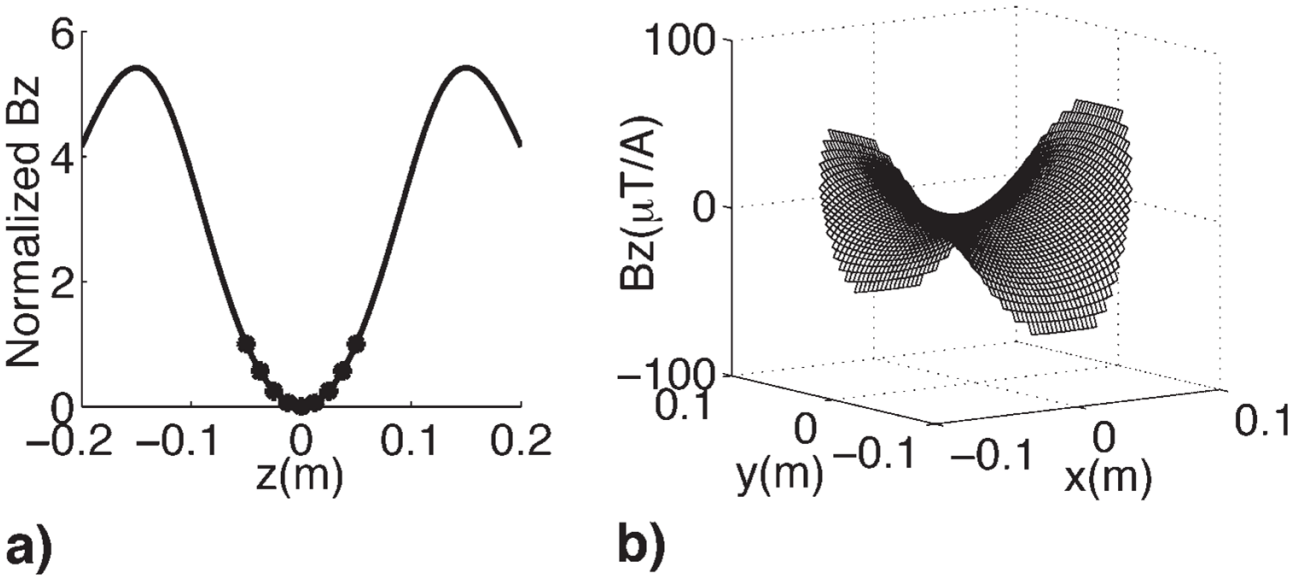

Figure 3.

(a) Magnetic field profile for Z^2, normalized to the edge of the region of interest, on the *z*-axis (solid line). (b) Calculated magnetic field profile in the *x* and *y* directions for the X^2–Y^2 shim coil with a radius of $a = 0.1$ m. For the Z^2 coil, the field targets (circles) were specified over a region of $z = \pm 0.5a$, the magnetic field profile meets the field targets within this region of interest. It can be seen that for this coil, quadratic behavior of the magnetic field continues well outside the region of interest.

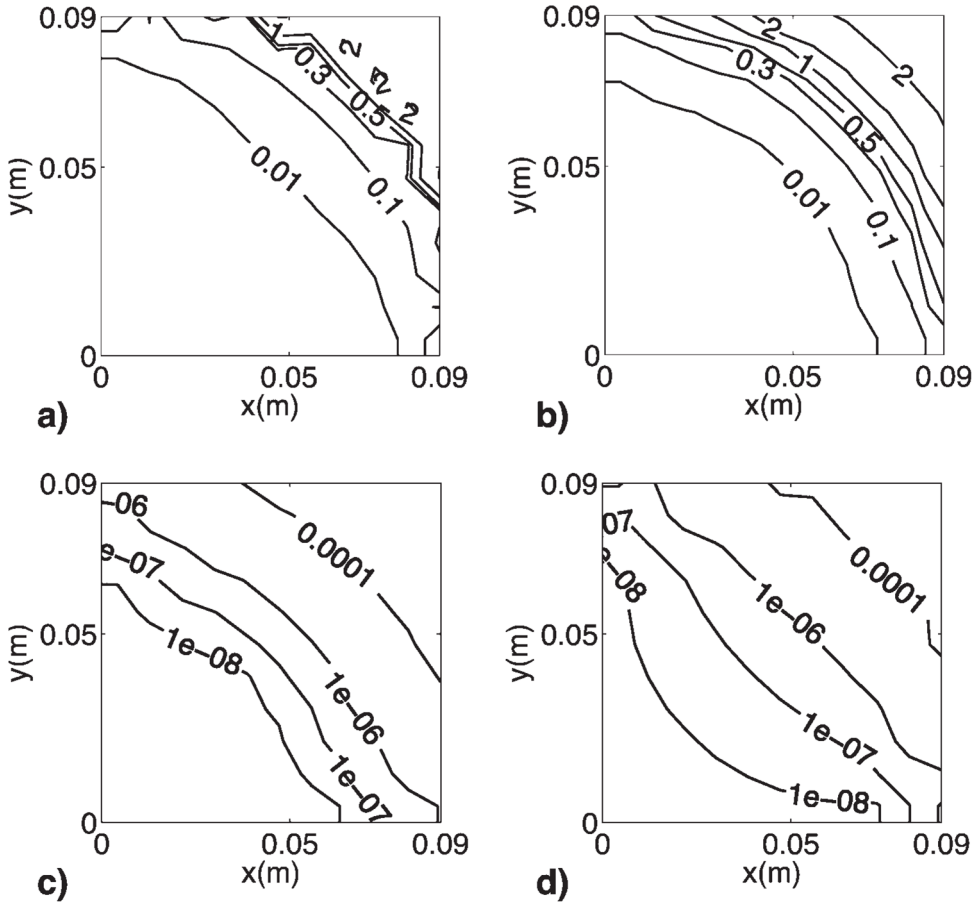

Figure 4.

One quadrant of the relative residual fields (top figures) and the absolute residual fields (bottom figures) in the *xy* plane for the X^2–Y^2 shim coils designed using minimum inductance (a, c) and minimum power methods (b, d). Within the ROI and in the *xy* plane, the average relative residual fields are <2% and the average absolute residual fields are $<10^{-7}$ T when evaluated using both design methods. The magnetic fields produced by the coils designed using minimum power and minimum inductance methods were scaled to have the same efficiency (17 $mT/m^2/A$).

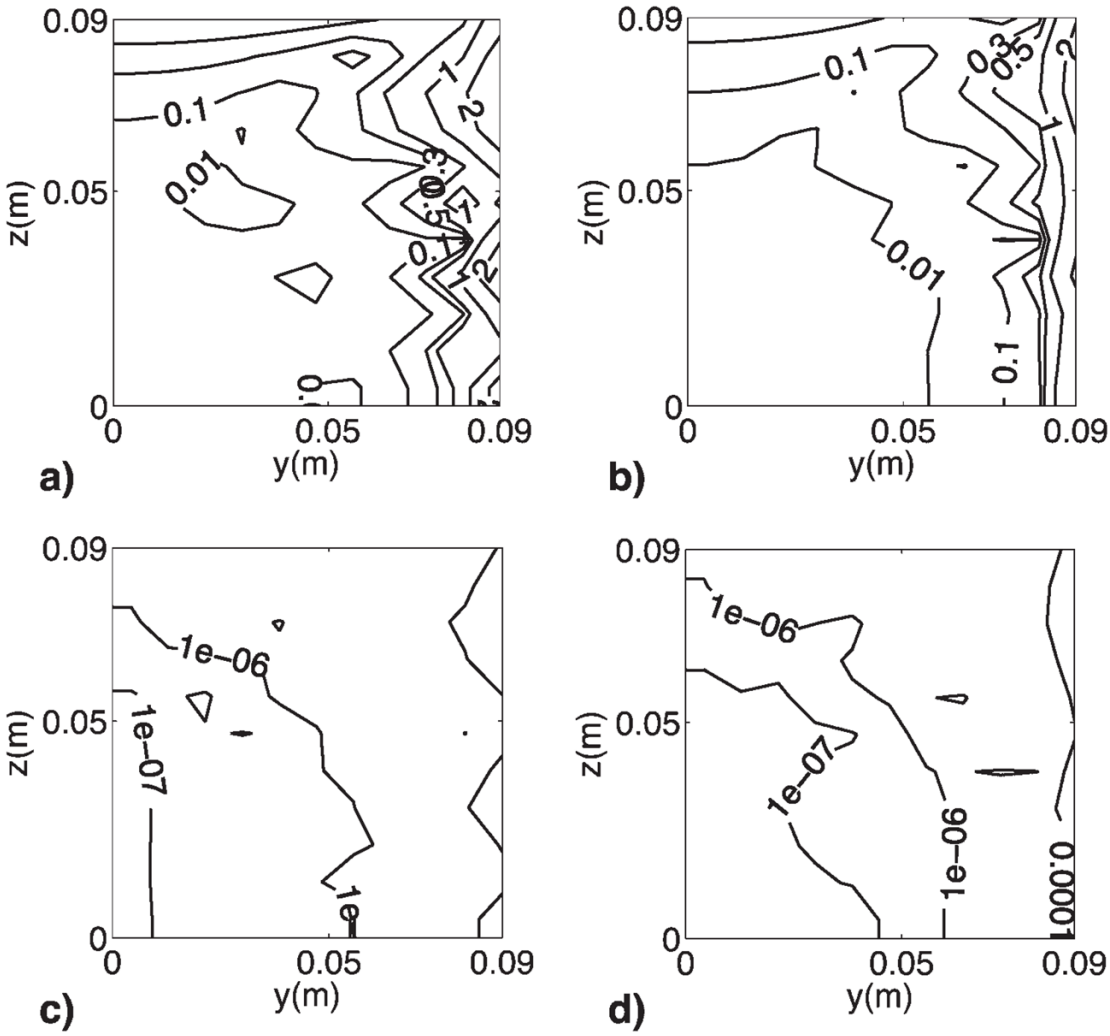

Figure 5.

One quadrant of the relative residual fields (top figures) and the absolute residual fields (bottom figures) in the *yz* plane for the X^2–Y^2 shim coils designed using minimum inductance (a, c) and minimum power methods (b, d). Within the ROI and in the *yz* plane, the average relative residual fields are <4% and the average absolute residual fields are $<10^{-6}$ T when evaluated using both design methods. The magnetic fields produced by the coils designed using minimum power and minimum inductance methods were scaled to have the same efficiency (17 mT/m^2/A).

Table 1

Performance Values for 10 Shim Axes Designed Using Minimum Inductance and Minimum Power Algorithms

		Inductive Merit			Resistive Merit		
Axis	**Analysis**	**Minimum Power Method**	**Minimum Inductance Method**	**Percent Difference**	**Minimum Power Method**	**Minimum Inductance Method**	**Percent Difference**
Z	Discrete	0.0957	0.101	5.40	0.00490	0.00460	6.32
	Continuous	0.0937	0.100	6.97	0.00620	0.00570	8.4
Z^2	Discrete	0.797	0.839	5.13	0.0373	0.0340	9.26
	Continuous	0.816	0.869	6.29	0.0462	0.0413	11.2
Z^3	Discrete	10.5	11.2	6.45	0.418	0.395	5.65
	Continuous	10.3	11.1	7.48	0.545	0.505	7.61
Z^4	Discrete	91.5	93.4	5.50	3.3282	3.0998	7.10
	Continuous	88.2	90.4	6.25	4.41	4.01	9.50
X and Y	Discrete	0.0870	0.0921	5.69	0.00400	0.00350	13.3
	Continuous	0.0879	0.0933	5.96	0.00520	0.00450	14.4
XY and $X^2–Y^2$	Discrete	1.53	1.63	6.33	0.0589	0.0535	9.6
	Continuous	1.53	1.62	5.71	0.0799	0.0718	10.7
YZ and XZ	Discrete	2.14	2.34	8.93	0.0625	0.0581	7.29
	Continuous	2.17	2.33	7.11	0.0844	0.0752	11.53

In every design case, the improvement in ML provided by the minimum inductance method is <10% of the value obtained using the minimum power method and the improvements in MR provided by the minimum power method are <15% of the values obtained using the minimum inductance method. The merit of inductance calculated with the discrete method agrees with the merit of inductance calculated with the continuous method within 3.5% in all cases. The difference between the merits of power calculated with the discrete and the continuous methods ranges between 10% and 30%.

Concepts Magn Reson Part B Magn Reson Eng. Author manuscript; available in PMC 2010 April 20.